

## Appendix A: RbLi: the good, the bad and the ugly

This appendix summarizes the best and the worst aspects of the RbLi apparatus. Hopefully the items presented here are helpful to future students building experimental apparatuses for ultracold atoms.

### A.1 The good

It is very easy to come up with a list of bad things that don't work quite well in the lab. Coming up with a list of good things that work well is harder; if we are not fixing a broken thing we don't think much about it. When the current postdoc was prompted with the question of what she loved most about our apparatus she answered 'I love every single thing about RbLi.' Unfortunately there is not enough space to talk about every single thing and the list below summarizes some good things in our lab.

**Overkill transistor banks:** Large currents in the lab (quadrupole and Zeeman slower) are controlled with MOSFET banks formed by a group of MOSFETS whose drain and source are connected in parallel and sharing the same gate voltage that is controlled by a PI servo. The Zeeman slower always operates at a fixed current but the current in the quadrupole coils is dynamically changed throughout the experimental sequence and a fast response is desirable. In 2013 we replaced the quadrupole MOSFET bank with a new unit that contains 20 IXFN 520N075T2 transistors rated for 75 V and 480 A. Even though our currents never exceed 70 A, the performance of the transistors really decays as the drain to source voltage is increased as can be seen in Figure 1. The use of more transistors reduces the power dissipation of each individual transistor which allows us to operate the power supply at a higher voltage of 15 V that helps counteract the inductive kickback of the coils. With the new transistor bank the turn on time of the coils was reduced from 100 ms to 50 ms leading to improved magnetic trapping and better Stern-Gerlach pulses for imaging, only with an unavoidable small number of blown off transistors.

**Hand made in vacuum shutters:** Before going into the Zeeman slower, the atoms that were heated in the Rb oven travel to the main oven chamber that is pictured in Figure 2b containing a cold-cup and an oven shutter. The cold-cup is a cylindrical shaped copper piece that is attached to the cold end of a thermo-electric cooler (TEC) via a copper rod. We keep the cold-cup temperature at  $-30\text{ C}$  in order to capture excess Rb atoms in the chamber and prevent damaging the ion pumps. The oven shutter allows us to block or enable the atomic beam. We use a homemade device, made from a re-purposed hard drive disk shutter with a

**Fig. 12. Forward-Bias Safe Operating Area**

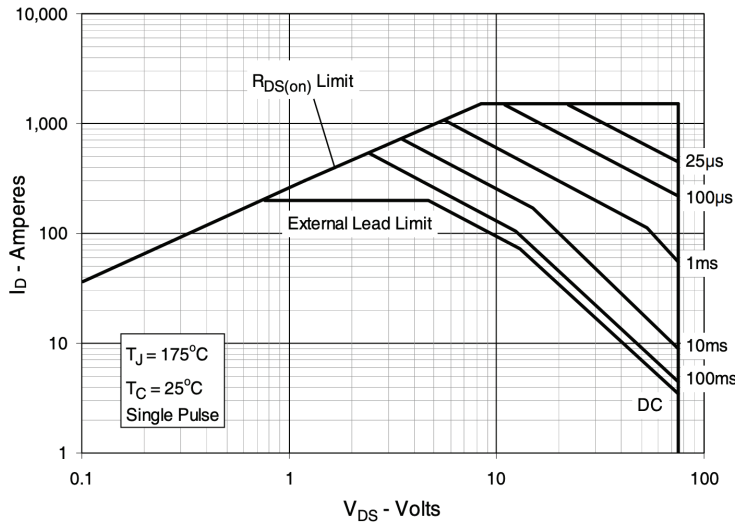


Figure 1: Safe operation regime of the IXFN 520N075T2 MOSFET. Even though they are in principle rated for up to 480 A the maximum safe current is greatly reduced at larger drain to source voltages  $V_{DS}$ . A high  $V_{DS}$  is desirable to reduce the inductive kickback during turn on.

metallic flag attached to its end. The shutter is electrically connected to an electric feedthrough with vacuum-compatible Kapton sealed wires. Other apparatus within the JQI [1,2] have commercial shutters from **Uniblitz** and some of them have failed in the past. Overall we have found this setup to be very reliable. The only problem we experienced once was some accumulation of Rb on the cold cup that started blocking the atomic beam. To remedy this we reversed the polarity of the TEC and heated the cold cup barely enough so that the accumulated Rb atoms melted and moved away from the aperture of the atomic beam.

**Ultraviolet LEDs:** We have two 3 W ultraviolet LEDs from **Mightex** placed at the glass cell side of the vacuum system. One is aimed at the vacuum window where the slower beam enters and the other is placed aiming at the glass cell. The LEDs prevent Rubidium from depositing on the vacuum system and can conveniently be turned on and off with a TTL signal from the computer. We have found that routinely turning them on (for example, leaving them on overnight) leads to a smoother operation of the system.

**Mirror mounts with picomotor actuators:** We use 8816-6 picomotor optical mounts from **New Focus Optics** whose deflection angle can be electronically adjusted on the order of microradians. The addition of picomotor mounts has made alignment of laser beams to the atoms significantly easier. We use these mounts on the last tunable mirror before the atoms for beam paths whose alignment is critical, for example in optical dipole trap and Raman beams.

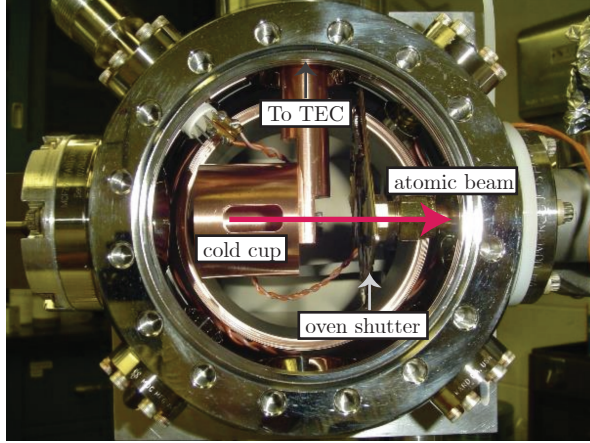


Figure 2:  $^{87}\text{Rb}$  level structure (not to scale). **a.** Ground and first excited state electronic configuration of  $^{87}\text{Rb}$  given by the  $\{n, \mathbf{L}\}$  quantum numbers. **b.** The interaction between the orbital angular momentum and the spin of the electron leads to the fine splitting of orbitals with  $L > 0$ . The splitting of the  $5^2P$  line gives rise to the D1 and D2 lines. **c.** The interaction between the total angular momentum and the nuclear spin causes the fine structure levels to split further into states characterized by the quantum number  $F$ .

**Stable polarization of MOT beams:** The light of our MOT beams is coupled to polarization maintaining optical fibers. We found that besides our best efforts to align the polarization of the incoming light to the axis of the fiber the fluctuations in the output polarization could cause considerable instabilities in the BEC production. To keep the polarization clean we placed polarizers at the output of the fibers. We found that despite the power hit we can get from the changes in polarization, this solution leads to a much more stable production of BECs.

**Lab couch:** When the experiment is functional enough that data can be taken long hours in the lab are often required. When it gets late, the lab couch allows the person running the experiment to take small breaks while experimental

**Others already mentioned in the main text:** The new master laser from Vescent photonics has been very stable and reliable. The new Mako camera has been very helpful to get rid of unwanted fringes in absorption images. Labscript makes writing experimental sequences very straightforward.

## A.2 The bad

**Free space dipole laser:** The laser system providing 1064 nm light for the optical dipole trap is not fiber coupled and is setup in the same optical table as the vacuum system; we are not able to change the laser without destroying the alignment of the beam with the atoms. This issue became important while setting up a 1D optical lattice by retro-reflecting one of the dipole trap beams we noticed that the laser mode is not very stable, leading to big fluctuations in the optical

lattice. In the original design of the laser system high-power photonic crystal fibers were included but they did not have built in mode expanders which resulted in the tip of the fiber inevitably getting burnt after some time of use. In short, mode expanders are recommended in applications involving large optical powers.

**Water cooling shared between two labs:** The quadrupole and Zeeman slower coils as well as the transistor banks require water cooling due to Joule heating. Our lab space is shared with a Rubidium-Ytterbium ultracold mixtures apparatus [3] and amongst the things we shared is the water cooling system. The schematic in Figure 3 illustrates the layout of the water cooling system. The water was filtered at two different points, first at each line has a  $440\text{ }\mu\text{m}$  particulate filter from Swagelok and then the water returning to the heat exchanger is filtered with a low-impedance cellulose cartridge (McMaster 7191K11). Both filters only capture impurities in the water for one given flow direction. One of the failure modes which occurs when one of the booster pumps is turned on before the heat exchanger, causing water to flow from one experiment to the other and bringing a collection of nasty things that escapes the filters into the coils. Over the years our system has suffered of clogged filters, clogged coils and broken booster pumps. For best operation it is highly recommended that the cartridge filter is changed and that the Swagelok filters be cleanned at least once a year and that a 10% solution of an anti-corrosive Optishield Plus in water is used as a coolant. Even when following this practices, we managed to find lots of gunk and unidentified objects (sand? glass? mud? oxide? dead bacteria?) in the water, it just accumulated at a slower rate.

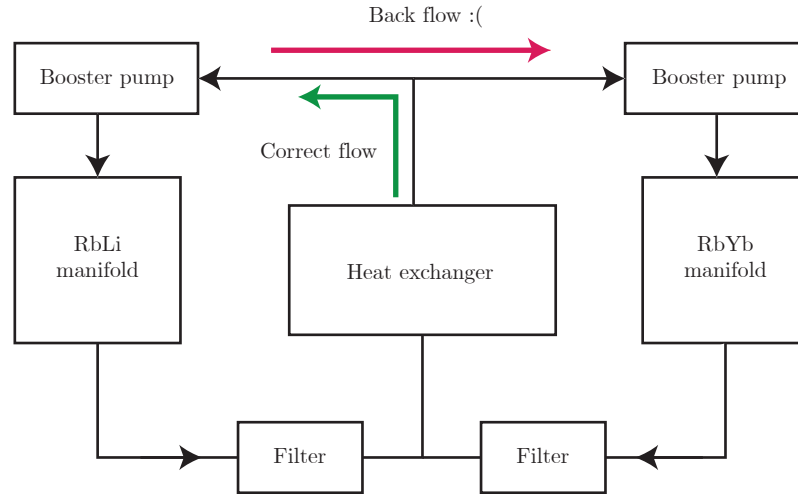


Figure 3: Simplified schematic of the shared water cooling manifold.

### A.3 The ugly

The ugly elements are not quite bad but they don't function flawlessly either.  
If given the option to replace them with something better I definitely would.

kepcos BoosTA too many NI usb devices on the same computer

## Appendix B: New apparatus

B.1 Water cooling stuff

B.2 Electrical installation

B.3 New Rb ‘oven’

## Appendix C: Full derivation of the Raman coupled $|xyz\rangle$ states

In this Appendix I derive the full time-dependent Hamiltonian describing the Raman coupled  $|xyz\rangle$  states. The system is based on the theoretical proposal in [4] to engineer an effective Rashba-type Hamiltonian using three Raman laser beams.

We consider an  $F = 1$  system that is subject to a constant magnetic field  $B_0 \mathbf{e}_z$  and an RF magnetic field  $B_{RF} \cos(\omega_{RF}t) \mathbf{e}_x$ . The system is described by the Hamiltonian

$$\hat{H}_{RF} = \omega_0 \hat{F}_z - \frac{\epsilon}{\hbar} (\hat{F}_z^2 - \mathbb{I}) + 2\Omega_{RF} \cos(\omega_{RF}t) \hat{F}_x, \quad (\text{C.1})$$

where  $\omega_0 = g_F \mu_B B_0$  is the Larmor frequency,  $\epsilon$  is a quadratic Zeeman shift that breaks the degeneracy of the  $|m_F = -1\rangle \leftrightarrow |m_F = 0\rangle$  and  $|m_F = 1\rangle \leftrightarrow |m_F = 0\rangle$  transitions, and  $\Omega_{RF} = g_F \mu_B B_{RF}/2$  is the RF coupling strength. We then transform the Hamiltonian into a rotating frame using the unitary transformation  $\hat{U}(t) = \exp(-i\omega_{RF}t \hat{F}_z)$ . The spin-1 operators under this transformation are transformed as

$$\begin{aligned} \hat{F}_x &\rightarrow \cos(\omega_{RF}t) \hat{F}_x - \sin(\omega_{RF}t) \hat{F}_y \\ &= e^{i\omega_{RF}t} \hat{F}_+ + e^{-i\omega_{RF}t} \hat{F}_- \\ \hat{F}_y &\rightarrow \sin(\omega_{RF}t) \hat{F}_x + \cos(\omega_{RF}t) \hat{F}_y \\ &= \frac{1}{i} (e^{i\omega_{RF}t} \hat{F}_+ - e^{-i\omega_{RF}t} \hat{F}_-) \\ \hat{F}_z &\rightarrow \hat{F}_z. \end{aligned} \quad (\text{C.2})$$

The unitary evolution in the rotating frame is described by the transformed Hamiltonian  $\hat{U}^\dagger(t)(\hat{H}_{RF} - i\hbar\partial_t)\hat{U}(t)$ , which after neglecting terms that are oscillating at  $2\omega_{RF}$  is

$$\hat{H}_{RWA} = \Delta \hat{F}_z - \frac{\epsilon}{\hbar} (\hat{F}_z^2 - \mathbb{I}) + \Omega_{RF} \hat{F}_x \quad (\text{C.3})$$

The eigenstate of Equation C.3 are the  $|xyz\rangle$  states described in Chapter ???. I will show later that all states can be coupled using a combination of the  $\hat{F}_x$ ,  $\hat{F}_y$ , and  $\hat{F}_z$  operators in the lab frame, i.e. using different combinations of Raman laser beams with appropriately chosen polarizations.

For simplicity I will start this description in the lab frame and I will not make any initial assumptions about direction of propagation or frequency each of the beams. Consider three linearly polarized Raman beams propagating along the  $xy$  plane as shown in Fig. 1. The electric field at the atoms is

$$\mathbf{E}(x, t) = \sum_{i=1}^3 E_i \mathbf{e}_i e^{i(\mathbf{k}_i \cdot \mathbf{x} - \omega_i t)}, \quad (\text{C.4})$$

where  $E_i$  is the field amplitude,  $\omega_i$  is the angular frequency, and  $\mathbf{e}_i$  is the polarization of each of the beams. In order to generate the necessary Raman couplings proportional to  $\hat{F}_x$ ,  $\hat{F}_y$  and  $\hat{F}_z$  we need two horizontally polarized Raman beams and one vertically polarized beam. Without loss of generality we choose

$$\begin{aligned} \mathbf{e}_1 &= \frac{(k_{1y}, -k_{1x}, 0)}{\|\mathbf{k}_1\|^2}, \\ \mathbf{e}_2 &= (0, 0, 1), \\ \mathbf{e}_3 &= \frac{(k_{3y}, -k_{3x}, 0)}{\|\mathbf{k}_3\|^2}, \end{aligned} \quad (\text{C.5})$$

The Raman Hamiltonian is given by the vector component of the Stark shift generated by the atom-light interaction

$$\hat{H}_R = (iu_v \mathbf{E} \times \mathbf{E}^*) \cdot \hat{F}, \quad (\text{C.6})$$

where  $u_v$  is the vector polarizability. Now let's expand Eq. C.6 using the field at the atoms from Eq. C.4.

$$\begin{aligned} \mathbf{E} \times \mathbf{E}^* &= (E_1^* \mathbf{e}_1 e^{-i(\mathbf{k}_1 \cdot \mathbf{x} - \omega_1 t)} + E_2^* \mathbf{e}_2 e^{-i(\mathbf{k}_2 \cdot \mathbf{x} - \omega_2 t)} + E_3^* \mathbf{e}_3 e^{-i(\mathbf{k}_3 \cdot \mathbf{x} - \omega_3 t)}) \times c.c \\ &= E_1^* E_2 (\mathbf{e}_1 \times \mathbf{e}_2) e^{i[(\mathbf{k}_2 - \mathbf{k}_1) \cdot \mathbf{x} - (\omega_2 - \omega_1)t]} + E_1^* E_3 (\mathbf{e}_1 \times \mathbf{e}_3) e^{i[(\mathbf{k}_3 - \mathbf{k}_1) \cdot \mathbf{x} - (\omega_3 - \omega_1)t]} \\ &\quad + E_2^* E_1 (\mathbf{e}_2 \times \mathbf{e}_1) e^{i[(\mathbf{k}_1 - \mathbf{k}_2) \cdot \mathbf{x} - (\omega_1 - \omega_2)t]} + E_2^* E_3 (\mathbf{e}_2 \times \mathbf{e}_3) e^{i[(\mathbf{k}_3 - \mathbf{k}_2) \cdot \mathbf{x} - (\omega_3 - \omega_2)t]} \\ &\quad + E_3^* E_1 (\mathbf{e}_3 \times \mathbf{e}_1) e^{i[(\mathbf{k}_1 - \mathbf{k}_3) \cdot \mathbf{x} - (\omega_1 - \omega_3)t]} + E_3^* E_2 (\mathbf{e}_3 \times \mathbf{e}_2) e^{i[(\mathbf{k}_2 - \mathbf{k}_3) \cdot \mathbf{x} - (\omega_2 - \omega_3)t]} \\ &= 2i \left[ (\mathbf{e}_1 \times \mathbf{e}_2) \text{Im}\{E_1^* E_2 e^{i(\mathbf{k}_{21} \cdot \mathbf{x} - \omega_{21}t)}\} \right. \\ &\quad + (\mathbf{e}_1 \times \mathbf{e}_3) \text{Im}\{E_1^* E_3 e^{i(\mathbf{k}_{32} \cdot \mathbf{x} - \omega_{32}t)}\} \\ &\quad \left. + (\mathbf{e}_2 \times \mathbf{e}_3) \text{Im}\{E_2^* E_3 e^{i(\mathbf{k}_{32} \cdot \mathbf{x} - \omega_{32}t)}\} \right] \end{aligned} \quad (\text{C.7})$$

also from the definitions of the polarization vectors we can calculate the cross products

$$\begin{aligned} \mathbf{e}_1 \times \mathbf{e}_2 &= \frac{(-k_{1x}, -k_{1y}, 0)}{\|\mathbf{k}_1\|^2} = -\hat{\mathbf{k}}_1 \\ \mathbf{e}_1 \times \mathbf{e}_3 &= \frac{(0, 0, -k_{1y}k_{3x} + k_{3y}k_{1x})}{\|\mathbf{k}_1\|^2 \|\mathbf{k}_3\|^2} = \mathbf{e}_z \sin \theta_{13} \\ \mathbf{e}_2 \times \mathbf{e}_3 &= \frac{(k_{3x}, k_{3y}, 0)}{\|\mathbf{k}_3\|^2} = \hat{\mathbf{k}}_3, \end{aligned} \quad (\text{C.8})$$

and putting everything together

$$\begin{aligned} iu_v \mathbf{E}^* \times \mathbf{E} \cdot \hat{\mathbf{F}} &= -2u_v \left[ -\hat{\mathbf{k}}_1 \text{Im}\{12\} + \mathbf{e}_z \sin \theta_{13} \text{Im}\{13\} + \hat{\mathbf{k}}_3 \text{Im}\{23\} \right] \cdot \hat{\mathbf{F}} \\ &= (\Omega_x, \Omega_y, \Omega_z) \cdot \hat{\mathbf{F}} \end{aligned} \quad (\text{C.9})$$

with

$$\begin{aligned} \Omega_x &= \frac{k_{1x}}{\|\mathbf{k}_1\|} \text{Im}\{\Omega_{12} e^{i(\mathbf{k}_{21} \cdot \mathbf{x} - \omega_{21} t)}\} + \frac{k_{3x}}{\|\mathbf{k}_3\|} \text{Im}\{\Omega_{23} e^{i(\mathbf{k}_{32} \cdot \mathbf{x} - \omega_{32} t)}\} \\ \Omega_y &= \frac{k_{1y}}{\|\mathbf{k}_1\|} \text{Im}\{\Omega_{12} e^{i(\mathbf{k}_{21} \cdot \mathbf{x} - \omega_{21} t)}\} + \frac{k_{3y}}{\|\mathbf{k}_3\|} \text{Im}\{\Omega_{23} e^{i(\mathbf{k}_{32} \cdot \mathbf{x} - \omega_{32} t)}\} \\ \Omega_z &= \text{Im}\{\Omega_{13} e^{i(\mathbf{k}_{31} \cdot \mathbf{x} - \omega_{31} t)}\}, \end{aligned} \quad (\text{C.10})$$

and

$$\begin{aligned} \Omega_{12} &= 2u_v E_1^* E_2 \\ \Omega_{13} &= -2u_v E_1^* E_3 \sin \theta_{13} \\ \Omega_{23} &= -2u_v E_2^* E_3. \end{aligned} \quad (\text{C.11})$$

#### C.0.0.1 Going into rotating frame

This is where things start getting fun. We need to transform Eq. C.9 into the rotating frame. Which terms are ‘slow’ and we get to keep and which are ‘fast’ depends on the specific choice of Raman frequencies. Only the  $\hat{F}_x$  and  $\hat{F}_y$  operators are affected by the unitary transformation while  $\hat{F}_z$  remains unchanged. We therefore choose the beams that give a  $\hat{F}_z$  coupling to be close in frequency.

There are two different frequency choices which Dan calls ‘blue’ and ‘red’ detuned which are shown in Fig. 2, and they determine whether  $\omega_{21}$  and  $\omega_{31}$  are positive or negative. I’m not sure if we can generalize something at this point. Lets look at the first term of the  $\Omega_x \hat{F}_x$  coupling for practice.

$$\begin{aligned} \Omega_x^{(1)} \hat{F}_x &\rightarrow \frac{1}{4i} \frac{k_{1x}}{\|\mathbf{k}_1\|} \left( \Omega_{12} e^{i(\mathbf{k}_{21} \cdot \mathbf{x} - \omega_{21} t)} - \Omega_{12}^* e^{-i(\mathbf{k}_{21} \cdot \mathbf{x} - \omega_{21} t)} \right) \left( e^{i\omega_{RF} t} \hat{F}_+ + e^{-i\omega_{RF} t} \hat{F}_- \right) \\ &\approx \frac{1}{4i} \frac{k_{1x}}{\|\mathbf{k}_1\|} \left( \Omega_{12} e^{i(\mathbf{k}_{21} \cdot \mathbf{x} - (\omega_{21} \mp \omega_{RF}) t)} \hat{F}_\pm - \Omega_{12}^* e^{-i(\mathbf{k}_{21} \cdot \mathbf{x} - (\omega_{21} \mp \omega_{RF}) t)} \hat{F}_\mp \right) \\ &= \frac{1}{4i} \frac{k_{1x}}{\|\mathbf{k}_1\|} \left( \Omega_{12} e^{i(\mathbf{k}_{21} \cdot \mathbf{x} - (\omega_{21} \mp \omega_{RF}) t)} - c.c. \right) \hat{F}_x \pm i \left( \Omega_{12} e^{i(\mathbf{k}_{21} \cdot \mathbf{x} - (\omega_{21} \mp \omega_{RF}) t)} + c.c. \right) \hat{F}_y \\ &= \frac{1}{2} \frac{k_{1x}}{\|\mathbf{k}_1\|} |\Omega_{12}| \left( \sin[\mathbf{k}_{21} \cdot \mathbf{x} - (\omega_{21} \mp \omega_{RF}) t + \phi_{12}] \hat{F}_x \pm \cos[\mathbf{k}_{21} \cdot \mathbf{x} - (\omega_{21} \mp \omega_{RF}) t + \phi_{12}] \hat{F}_y \right) \end{aligned} \quad (\text{C.12})$$

Where the upper sign corresponds to the  $\omega_{21} > 0$  case (blue detuned) and the lower

sign to  $\omega_{21} < 0$  (red detuned). Similarly, the second therm of  $\Omega_x \hat{F}_x$  is

$$\begin{aligned}\Omega_x^{(2)} \hat{F}_x &\rightarrow \frac{1}{4i} \frac{k_{3x}}{\|\mathbf{k}_3\|} (\Omega_{23} e^{i(\mathbf{k}_{32} \cdot \mathbf{x} - \omega_{32})t} - \Omega_{23}^* e^{-i(\mathbf{k}_{32} \cdot \mathbf{x} - \omega_{32}t)}) (e^{i\omega_{RF}t} \hat{F}_+ + e^{-i\omega_{RF}t} \hat{F}_-) \\ &\approx \frac{1}{2} \frac{k_{3x}}{\|\mathbf{k}_3\|} |\Omega_{23}| (\sin[\mathbf{k}_{32} \cdot \mathbf{x} - (\omega_{32} \mp \omega_{RF})t + \phi_{23}] \hat{F}_x \pm \cos[\mathbf{k}_{32} \cdot \mathbf{x} - (\omega_{32} \mp \omega_{RF})t + \phi_{23}] \hat{F}_y)\end{aligned}\quad (C.13)$$

where I used the same sign convention as before. It is important to keep in mind though that if  $\omega_{21}$  is positive then  $\omega_{32}$  must be negative and vice versa. **Double check again that signs are correct!** Let's continue with the algebra galore...

$$\begin{aligned}\Omega_y^{(1)} \hat{F}_y &\rightarrow -\frac{1}{4} \frac{k_{1y}}{\|\mathbf{k}_1\|} (\Omega_{12} e^{i(\mathbf{k}_{21} \cdot \mathbf{x} - \omega_{21}t)} - \Omega_{12}^* e^{-i(\mathbf{k}_{21} \cdot \mathbf{x} - \omega_{21}t)}) (e^{i\omega_{RF}t} \hat{F}_+ - e^{-i\omega_{RF}t} \hat{F}_-) \\ &= \mp \frac{1}{4} \frac{k_{1y}}{\|\mathbf{k}_1\|} (\Omega_{12} e^{i(\mathbf{k}_{21} \cdot \mathbf{x} - (\omega_{21} \mp \omega_{RF})t)} \hat{F}_\pm + \Omega_{12}^* e^{-i(\mathbf{k}_{21} \cdot \mathbf{x} - (\omega_{21} \mp \omega_{RF})t)} \hat{F}_\mp) \\ &= \mp \frac{1}{4} \frac{k_{1y}}{\|\mathbf{k}_1\|} ((\Omega_{12} e^{i(\mathbf{k}_{21} \cdot \mathbf{x} - (\omega_{21} \mp \omega_{RF})t)} + c.c.) \hat{F}_x + i (\Omega_{12} e^{i(\mathbf{k}_{21} \cdot \mathbf{x} - (\omega_{21} \mp \omega_{RF})t)} - c.c.) \hat{F}_y) \\ &= \mp \frac{1}{2} \frac{k_{1y}}{\|\mathbf{k}_1\|} |\Omega_{12}| (\cos[\mathbf{k}_{21} \cdot \mathbf{x} - (\omega_{21} \mp \omega_{RF})t + \phi_{12}] \hat{F}_x - \sin[\mathbf{k}_{21} \cdot \mathbf{x} - (\omega_{21} \mp \omega_{RF})t + \phi_{12}] \hat{F}_y)\end{aligned}\quad (C.14)$$

and

$$\begin{aligned}\Omega_y^{(2)} \hat{F}_y &\rightarrow -\frac{1}{4} \frac{k_{3y}}{\|\mathbf{k}_3\|} (\Omega_{23} e^{i(\mathbf{k}_{32} \cdot \mathbf{x} - \omega_{32}t)} - \Omega_{23}^* e^{-i(\mathbf{k}_{32} \cdot \mathbf{x} - \omega_{32}t)}) (e^{i\omega_{RF}t} \hat{F}_+ - e^{-i\omega_{RF}t} \hat{F}_-) \\ &\approx \mp \frac{1}{2} \frac{k_{3y}}{\|\mathbf{k}_3\|} |\Omega_{23}| (\cos[\mathbf{k}_{32} \cdot \mathbf{x} - (\omega_{32} \mp \omega_{RF})t + \phi_{23}] \hat{F}_x - \sin[\mathbf{k}_{32} \cdot \mathbf{x} - (\omega_{32} \mp \omega_{RF})t + \phi_{23}] \hat{F}_y)\end{aligned}\quad (C.15)$$

The complete Hamiltonian in the rotating frame after doing the rotating wave ap-

proximation is then

$$\begin{aligned}
\hat{H} = & \frac{1}{2} \frac{|\Omega_{12}|}{||\mathbf{k}_1||} \left( \left( k_{1x} \sin[\mathbf{k}_{21} \cdot \mathbf{x} - (\omega_{21} \mp \omega_{RF})t + \phi_{12}] \pm k_{1y} \cos[\mathbf{k}_{21} \cdot \mathbf{x} - (\omega_{21} \pm \omega_{RF})t + \phi_{12}] \right) \hat{F}_x \right. \\
& + \left. \left( \pm k_{1x} \cos[\mathbf{k}_{21} \cdot \mathbf{x} - (\omega_{21} \mp \omega_{RF})t + \phi_{12}] \mp k_{1y} \sin[\mathbf{k}_{21} \cdot \mathbf{x} - (\omega_{21} \pm \omega_{RF})t + \phi_{12}] \right) \hat{F}_y \right) \\
& \frac{1}{2} \frac{|\Omega_{23}|}{||\mathbf{k}_3||} \left( \left( k_{3x} \sin[\mathbf{k}_{32} \cdot \mathbf{x} - (\omega_{32} \mp \omega_{RF})t + \phi_{23}] \pm k_{3y} \cos[\mathbf{k}_{32} \cdot \mathbf{x} - (\omega_{32} \pm \omega_{RF})t + \phi_{23}] \right) \hat{F}_x \right. \\
& + \left. \left( \pm k_{3x} \cos[\mathbf{k}_{32} \cdot \mathbf{x} - (\omega_{32} \mp \omega_{RF})t + \phi_{23}] \mp k_{3y} \sin[\mathbf{k}_{32} \cdot \mathbf{x} - (\omega_{32} \pm \omega_{RF})t + \phi_{23}] \right) \hat{F}_y \right) \\
& + |\Omega_{13}| \sin(\mathbf{k}_{31} \cdot \mathbf{x} - \omega_{31}t + \phi_{13}) \hat{F}_z
\end{aligned} \tag{C.16}$$

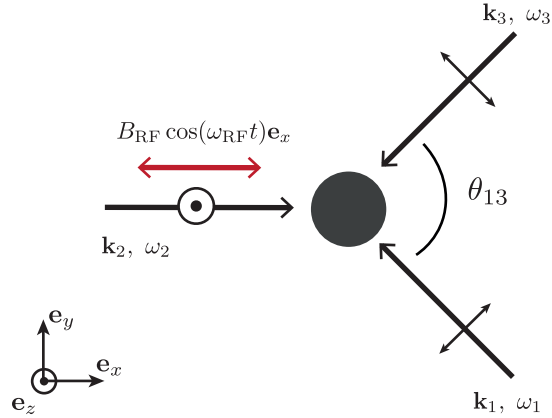


Figure 1: Laser layout: We use a strong RF field and three linearly polarized Raman beams propagating in the  $xy$  plane couple the  $|xyz\rangle$  states and engineer the Rashba Hamiltonian.

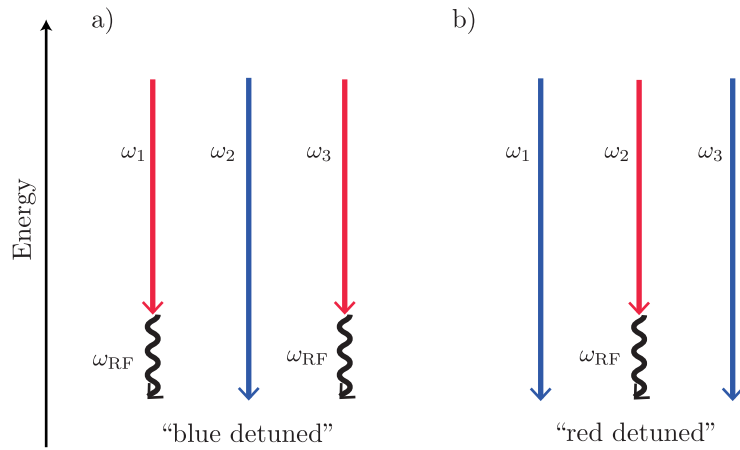


Figure 2: Laser frequencies: We have two frequency choices that allow us to address the three transitions between the  $|xyz\rangle$  states. **a)** The blue detuned case. There are 2 frequencies smaller by about  $\omega_{RF}$  and one larger frequency. **b)** The red detuned case. There are 2 frequencies that are larger by about  $\omega_{RF}$  and one smaller frequency. Nice!

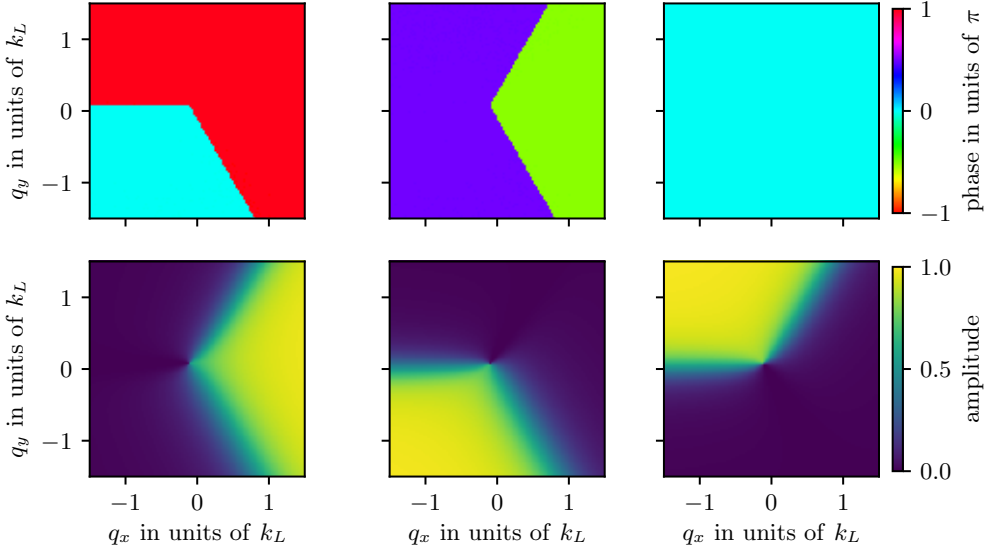


Figure 3: **a** Probabilities as a function of quasimomentum for the three output ports of the interferometer at  $t_{\text{free}} = 160 \mu\text{s}$  **b** Probabilities as a function of free evolution time  $t_{\text{free}}$  for an input state with quasimomentum  $(q_1, q_2) = (0.55, -0.92) k_L$  indicated by the blue star on **a** and in the topological ground branch ( $n = 1$ )

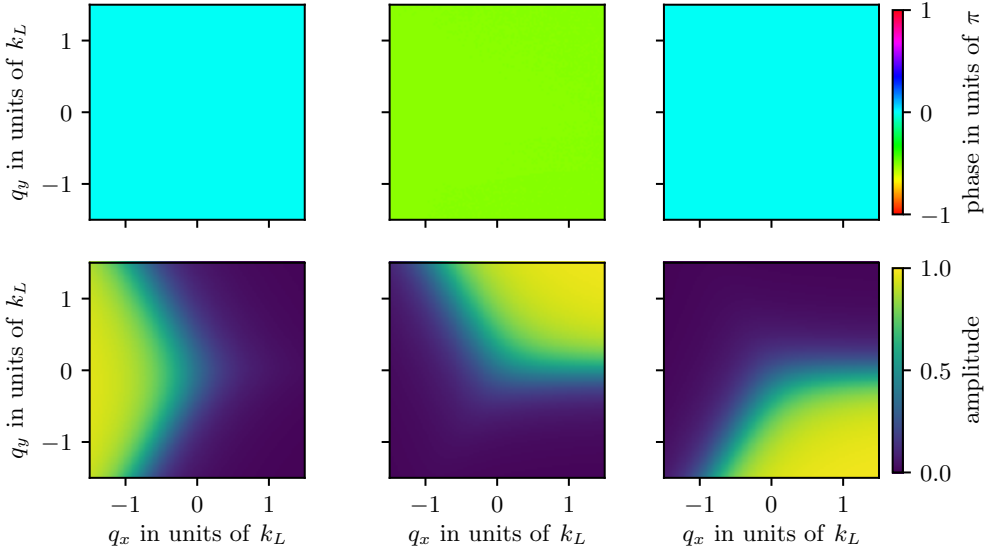


Figure 4: **a** Probabilities as a function of quasimomentum for the three output ports of the interferometer at  $t_{\text{free}} = 160 \mu\text{s}$  **b** Probabilities as a function of free evolution time  $t_{\text{free}}$  for an input state with quasimomentum  $(q_1, q_2) = (0.55, -0.92) k_L$  indicated by the blue star on **a** and in the topological ground branch ( $n = 1$ )

## Bibliography

- [1] Roger Brown. *Nonequilibrium many body dynamics with ultracold atoms in optical lattices and selected problems in atomic physics*. PhD thesis, University of Maryland College Park, Digital Repository at the University of Maryland, 6 2014.
- [2] K. Jiménez-García, L. J. LeBlanc, R. A. Williams, M. C. Beeler, A. R. Perry, and I. B. Spielman. Peierls substitution in an engineered lattice potential. *Phys. Rev. Lett.*, 108:225303, May 2012.
- [3] Creston D. Herold. *Ultracold mixtures of Rubidium and Ytterbium for open system quantum engineering*. PhD thesis, University of Maryland College Park, Digital Repository at the University of Maryland, 6 2014.
- [4] D. L. Campbell and I. B. Spielman. Rashba realization: Raman with RF. *New J. Phys.*, 18(3):033035, 2016.